Aerospace Science and Technology 22 (2012) 45–57

Contents lists available at ScienceDirect

Aerospace Science and Technology

www.elsevier.com/locate/aescte

Reduction of the actuator oscillations in a free–free jointed bipartite beam model under a follower force

O. Kavianipour [a,1], A.M. Khoshnood [b,*,1], S. Irani [c,2], J. Roshanian [c,3]

[a] Mechanical Engineering Faculty, Iran University of Science and Technology, PO Box: 16846-13114, Tehran, Iran
[b] Mechanical Engineering Faculty, K.N. Toosi University of Technology, PO Box: 19395-1999, Tehran, Iran
[c] Aerospace Engineering Faculty, K.N. Toosi University of Technology, PO Box: 16765-3381, Tehran, Iran

ARTICLE INFO

Article history:
Received 10 April 2010
Accepted 11 June 2011
Available online 30 June 2011

Keywords:
Two Stage to Orbit Launch Vehicle (TSTO LV)
Beam instability
Non-conservative force
Follower force
Adaptive algorithm
Notch filter

ABSTRACT

The flexible behaviors in the aerospace structures can lead to undesired performance and degradation of their control and guidance system. The aims of the current work are to analyze the bending vibration of a Two Stage to Orbit (TSTO) Launch Vehicle (LV) with propulsion force modeled as a free–free jointed bipartite beam under a follower force, study its effects on oscillation of the actuators, and finally develop a solution to reduce these oscillations. The vibration analysis of the beam model is carried out using Ritz method. The rigid dynamics of a TSTO LV in the pitch channel was then modeled and modified using the vibrational model of the device for the same channel. A new dynamic model with an adaptive control system for a TSTO LV has been developed, allowing the aerospace structure to run on its maximum bearable propulsion force with the optimum effects on the oscillation of its actuators. Simulation results show that such a control model provides an effective way to reduce the undesirable oscillations of the actuators.

1. Introduction

Many problems are modeled by beams subjected to axial or follower forces. The stability of the beams under the axial or follower force is of vital importance and is in interest of many researchers that can be applied to many aerospace structures where these forces represent the propulsion force. The direction of the axial force is assumed to be immovable while the direction of the follower force is always perpendicular to the cross surface of the beam and changes with the beam deflections. The critical axial force normally causes the static instability (divergence) and the follower force may cause static or dynamic instability (flutter). Divergence happens when the vibration frequency of the system becomes zero and flutter occurs when two natural frequencies of the systems converge together.

The current developments in the aerospace vehicles design have led to produce large flexible structures especially in the new launch vehicles. The bigger values of propulsion force-to-weight and length-to-diameter ratios required for long-range flights as well as the cost reduction of handling and launching operation lead to the highly Flexible Launch Vehicles (FLV). The dynamic response and vibrational characteristics of FLV are of vital importance. The TSTO LV structure is one of the important models for FLV and is studied as the core model in this paper. The TSTO LV structure is modeled by a jointed bipartite beam under the follower and transversal forces that is an acceptable model for such structures with propulsion and controller (actuator) forces (with the actuator forces responsible for the control and guidance of the TSTO LV). The separation and adapter interface equipment between stage 1 and 2 are modeled by two shear and rotational springs as shown in Fig. 1. The objective pursued in this study is to determine the maximum follower force structurally bearable in such a way as to prevent instability of the structure. On the other hand, flexibility and the elastic behaviors in the TSTO LV can lead to undesired performance and degradation of its control system due to influence of the body vibrations on the Inertial Measurement Units (IMU) measurements.

In the current work, the critical follower force for a TSTO LV model which leads to the instability has been calculated using Ritz method. The effect of the follower force on the vibration in the TSTO LV especially on its IMU is also investigated using Newmark and ode4 (Runge–Kutta Formula) methods. Also the destructive effect of the vibration of the IMU on oscillation of the TSTO LV

* Corresponding author.
E-mail addresses: o.kavianipour@gmail.com (O. Kavianipour), khoshnood@dena.kntu.ac.ir (A.M. Khoshnood), irani@kntu.ac.ir (S. Irani), roshanian@kntu.ac.ir (J. Roshanian).
[1] PhD student.
[2] Assistant professor, head of the Aerospace Structures Department. Tel.: +98 21 77791044; fax: +98 21 77791045.
[3] Associate professor.

1270-9638/$ – see front matter
doi:10.1016/j.ast.2011.06.001

Nomenclature

$(\ddot{\ldots})$	$d^2(\ldots)/d\bar{t}^2$
$(\ldots)'$	$d(\ldots)/d\bar{x}$
$(\ldots)''$	$d^2(\ldots)/d\bar{x}^2$
$(\ldots)'''$	$d^3(\ldots)/d\bar{x}^3$
$(\bar{\ldots})$	non-dimensional parameter for $(\ldots)$
$A_1, \ldots, A_8$	mode shape coefficients
a_i, b_j	constant coefficient in the transfer function
EI_1	bending stiffness of the first part of the beam
EI_2	bending stiffness of the second part of the beam
$F_0(t)$	transversal controller force applied at x_{F_0}
$g(n)$	output of the pole section
I	identity matrix
$\lfloor K_{ij} \rfloor$	stiffness matrix
$k_{cg}(n)$	correcting gain
k_r	stiffness of the rotational spring
k_s	stiffness of the shear spring
L_1	length of the first part of the beam
L_2	length of the second part of the beam
$\lfloor M_{ij} \rfloor$	mass matrix
m_1	mass per unit length of the first part of the beam
m_2	mass per unit length of the second part of the beam
P_0	follower force
P_{0cr}	critical follower force
P_1	axial force of the first part of the beam
P_2	axial force of the second part of the beam
$\lfloor Q_j \rfloor$	generalized force vector
$\lfloor \bar{q}_j \rfloor$	constant vector
$q_i(\bar{t})$	generalized coordinate
T	kinetic energy
t	time
$u(n)$	input of the first filter for eliminating the rigid body dynamic at the nth step
V	potential energy
W_c	work done by conservative forces
W_{nc}	work done by non-conservative forces
$w(n)$	output of the filter
$\hat{z}(n)$	estimated parameters matrix
α	a function of the center frequency of the filter
β	constant parameter
δ	variation sign
δ_p	actuator deflection of the pitch channel
$\varphi_i(\bar{x})$	admissible function
$\varphi_i'(x_{IMU})$	slope of the mode shape at the IMU location
$\eta(n)$	regression model of out put
λ_1	first natural frequency for $\bar{P}_0 = 0$
$\bar{\lambda}$	the non-dimensional frequency of the system with non-zero of $\bar{P}_0$
θ	pitch magnitude of a rigid beam
θ_b	magnitude of the bending angle
θ_T	total pitch magnitude
ω_i	the natural frequency of the free–free jointed bipartite beam
$\psi(n)$	recursive parameters

actuator in a control loop is presented. Finally an adaptive notch filter is designed and implemented by using filtered recursive least square (FRLS) method to develop a new dynamic model and an adaptive control system. The effectiveness of this system is discussed later in this paper.

Bokaian [5] obtained an analytical characteristic equation for uniform beams under constant compressive axial load and considered some approximate relations for the buckling load and variation of normalized natural frequency with normalized axial force. Joshi [14] established a simple method to determine the mode shapes and the natural frequencies of a non-uniform beam subjected to rear end propulsion force. Another research to obtain the governing vibration equations and the stability of a beam under axial force was carried out by Nihous [24]. Pourtakdoust and Assadian [28] modeled a free–free Bernoulli beam under an axial force. The three dimensional elastic equations of vibration are solved by FEM. Only the divergence instability was found and shown in their work. And finally the elastic equations beside the equations of motion were simulated in a controller loop by the authors in their last work. It was shown that the oscillations of the actuators were increased when the axial force was applied. Hassanpour et al. [11] analyzed the exact solution of free vibration of a beam with a concentrated mass within its intervals when the beam was subjected to axial loadings. They determined the exact mode shapes of vibration, which were required in the study of the time-domain response of sensors and determination of stability regions. Langthjem and Sugiyama [18] studied a cantilever beam under a follower force with a tip mass to optimize the design of the beam. Another research in instability of a non-uniform cantilever beam under a follower force was carried out by Au et al. [1] using finite element method. Langthjem and Sugiyama [19] offered a survey of simple, flexible structural elements subjected to non-conservative follower loads. Many researches were also published for cantilever beam under a follower force when the damping was considered such as Ryu and Sugiyama [30], Detinko [8], Egidio et al. [9] and Lee et al. [20]. Sugiyama and Langthjem [32] studied cantilever beam under a follower force with proportional damping. Both internal (material) and external (viscous fluid) damping were considered. Beal [2] investigated a uniform free–free beam under an end follower force. He introduced a direction control mechanism for the follower force to eliminate the tumbling instability of a free–free beam under a follower force. He also showed that, in the absence of the control system, the critical follower force magnitude is associated with coalescence of the two lowest bending frequencies. When the control system was included, it was found that the critical follower force magnitude only corresponded to a reduction of the lowest frequency of zero. Wu [33] studied the stability of a free–free beam under a controlled follower force by using finite element discretization with an adjoint formulation. Park and Mote Jr. [27] studied the maximum controlled follower force on a free–free beam carrying a concentrated mass. They predicted the location and the magnitude of the additional concentrated mass and the location and the gain of the follower force direction control sensor that permit the follower force to maximized for stable transverse motion of the beam. Park [26] investigated a uniform free–free Timoshenko beam under an end follower force with controlled direction. A finite element model of the beam transverse motion in the plane was formulated through the extended Hamilton's principle. The analysis showed that the effects of the rotary inertia and shear deformation parameters on the stable transverse motion of the beam are significant in certain ranges. Sato [31] developed the governing equation of motion of a Timoshenko beam under a follower force using Hamilton's principle. Mladenov and Sugiyama [23] dealt with the stability of a flexible space structure subjected to an end follower force. The model consisted of two viscoelastic beams interconnected by two kinds of joints. One of the joints was composed of a rotational viscoelastic spring while another one was a shear viscoelastic spring. Bending flutter or post-flutter di-

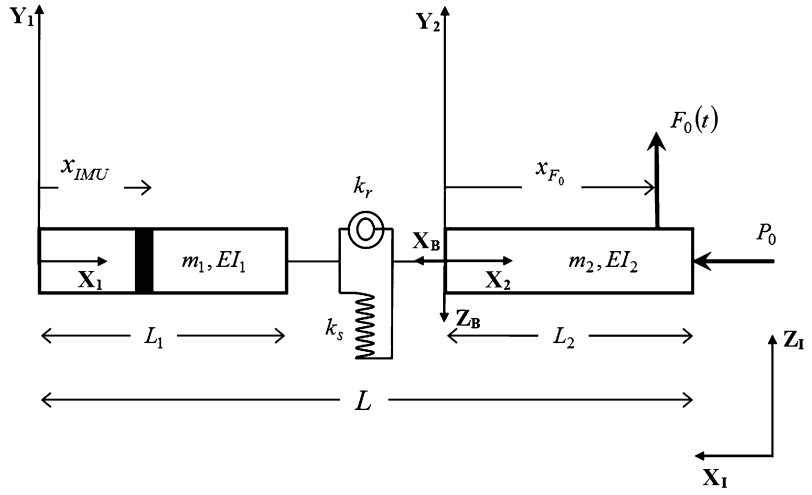

Fig. 1. The simple model of an aerospace structure as a jointed bipartite beam.

vergence showed to occur depending on the joint rigidity and the internal damping. Kim and Choo [17] analyzed the dynamic stability of a free–free Timoshenko beam with a concentrated mass subjected to a pulsating follower force. The effects of axial location and translation inertia of the concentrated mass were studied. The change of combination resonance types, the relationship between critical forces and widths of instability regions and the effect of shear deformation were also examined by them. Irani and Kavianipour [12] investigated effects of a flexible joint on instability of a free–free jointed bipartite beam under the follower and transversal forces. Kavianipour and Sadati [15] studied effects of damping on the linear stability of a free–free beam subjected to follower and transversal forces.

To reduce the undesired effects of vibration many researchers used optimized control methods in their design of the LV control systems such as Ryanski [29], Jenkins and Roy [13] and Maki et al. [21]. The optimized control methods included linear and nonlinear in the basis of the minimization of the generalized vibration modes. Bibel and Stalford [4,3] improved gain stabilized mu-controller as well as a control design for a flexible launch vehicle. Englehart and Krause [10] proposed an analogue notch filter with least square algorithm to reduce the bending vibrational effects on a LV. Choi and Bang [6], and Choi and Kim [7] also designed an adaptive control approach to the attitude control of a flexible aerospace system. They used the root mean square method to estimate the bending frequency and one digital notch filter to reduce the flexible behaviors, considering the first and the second bending vibration modes. Oh et al. [25] examined the attitude control of a flexible launch vehicle using an adaptive notch filter. In another work, Khoshnood et al. [16] proposed a model reference adaptive control for reducing the undesired effects of bending vibration for a LV. However the effects of follower force were not considered in their work.

This work essentially consists of two parts:

Part 1 includes the solution of the elastic equation of the structure in order to find the propulsion force bearable by the structure. With the particular solution method used (Ritz method), there is a need for the mode shapes for the free–free beam with a proportional damping.

Part 2 makes use of the linear model for the rigid–elastic body motion and includes the control system for decreasing the vibrations of the actuators.

These two parts are then combined in the end to perform a simulation of the overall controlled system.

2. Elastic equations

Fig. 1 shows the assumed model for the beam where two springs represent the joint of the two parts of the beam. The propulsion force is modeled by a follower force and the transverse force represents the controller force, as shown. Define the $Z_I X_I$, $Z_B X_B$, $Y_1 X_1$, and $Y_2 X_2$ as the inertial frame, body frame, and the elastic frame, respectively. The inertial frame is fixed and the body frame and elastic frame are attached to the beam. The mass of the structure is considered to be constant, with no translation of the center of mass of the whole structure. In spite of this, this analysis can be hold for mass variant systems. In Fig. 1, x_{IMU} and x_{F_0} are the sensors location (IMU) location and the controller force location respectively. The beam has been assumed to be axially rigid and is a Bernoulli beam. The gravity force is also ignored.

2.1. Energy considerations

One of the most effective methods to derive the governing equations is the Energy Method. In fact, by having all of the energies in the system and applying the Hamilton's Principle, the governing equations could be derived. The Hamilton's Principle can be expressed as [22]:

$$\delta \int_{t_1}^{t_2} (T - V + W_c)\,\mathrm{d}t + \int_{t_1}^{t_2} \delta W_{nc}\,\mathrm{d}t = 0 \tag{1}$$

where δ is the variation, t is time, T is the kinetic energy, V is the potential energy, W_c is the work done by conservative forces, and W_{nc} is the work done by non-conservative forces. For the presented model in Fig. 1, the above items could be presented as:

$$T = \frac{1}{2}\int_0^{L_1} m_1 \left(\frac{\partial y_1}{\partial t}\right)^2 \mathrm{d}x_1 + \frac{1}{2}\int_0^{L_2} m_2 \left(\frac{\partial y_2}{\partial t}\right)^2 \mathrm{d}x_2$$

$$V = \frac{1}{2}\int_0^{L_1} EI_1 \left(\frac{\partial^2 y_1}{\partial x_1^2}\right)^2 \mathrm{d}x_1 + \frac{1}{2}\int_0^{L_2} EI_2 \left(\frac{\partial^2 y_2}{\partial x_2^2}\right)^2 \mathrm{d}x_2 + \frac{1}{2}k_r \left(\left.\frac{\partial y_1}{\partial x_1}\right|_{x_1=L_1} - \left.\frac{\partial y_2}{\partial x_2}\right|_{x_2=0}\right)^2 + \frac{1}{2}k_s (y_1|_{x_1=L_1} - y_2|_{x_2=0})^2$$

$$W_c = \frac{1}{2}\int_0^{L_1} P_1\left(\frac{\partial y_1}{\partial x_1}\right)^2 \mathrm{d}x_1 + \frac{1}{2}\int_0^{L_2} P_2\left(\frac{\partial y_2}{\partial x_2}\right)^2 \mathrm{d}x_2$$

$$\delta W_{nc} = -P_0\left(\left.\frac{\partial y_2}{\partial x_2}\right|_{x_2=L_2}\right)\delta y_2|_{x_2=L_2} + F_0(t)\delta y_2|_{x_2=x_{F_0}} \tag{2}$$

where L_1, m_1, EI_1, P_1 are the length, mass per unit length, bending stiffness, and axial force of the first part of the beam respectively, and also L_2, m_2, EI_2, P_2 are the length, mass per unit length, bending stiffness, and axial force of the second part. k_r and k_s are the stiffness of the rotational and shear springs respectively. P_0 is the follower force and $F_0(t)$ is the transversal controller force applied at x_{F_0}.

To calculate the axial force along each part of the beam, the dynamics equilibrium can be used:

$$\begin{cases} P_1 = \dfrac{x_1}{L_1+L_2}P_0, & 0 \leqslant x_1 \leqslant L_1 \\ P_2 = \dfrac{L_1+x_2}{L_1+L_2}P_0, & 0 \leqslant x_2 \leqslant L_2 \end{cases} \tag{3}$$

As the effects of the bending stiffness are not in the interest of this study and mostly the effects of stiffness and the joint location is considered. It has been assumed that the two parts of the beam are uniform and have similar characteristics and:

$$m_1 = m_2 = m, \qquad EI_1 = EI_2 = EI \tag{4}$$

The dimension of the joint itself is assumed to be small and is neglected, so:

$$L_1 + L_2 = L \tag{5}$$

To simplify the equations, non-dimensional parameters are introduced as following:

$$\begin{aligned} &\bar{x}_1 = \frac{x_1}{L}, \qquad \bar{x}_2 = \frac{x_2}{L} \\ &\bar{y}_1 = \frac{y_1}{L}, \qquad \bar{y}_2 = \frac{y_2}{L} \\ &\bar{L}_1 = \frac{L_1}{L}, \qquad \bar{t} = t\left(\frac{EI}{mL^4}\right)^{0.5} \\ &\bar{k}_r = \frac{k_r L}{EI}, \qquad \bar{k}_s = \frac{k_s L^3}{EI} \\ &\bar{P}_0 = \frac{P_0 L^2}{EI}, \qquad \bar{F}_0 = \frac{F_0 L^2}{EI} \end{aligned} \tag{6}$$

If Eqs. (3), (4), (5) and (6) are replaced in Eqs. (1) and (2), then one could reach the following:

$$\delta\int_{\bar{t}_1}^{\bar{t}_2} (\bar{T} - \bar{V} + \bar{W}_c)\,\mathrm{d}\bar{t} + \int_{\bar{t}_1}^{\bar{t}_2} \delta\bar{W}_{nc}\,\mathrm{d}\bar{t} = 0 \tag{7}$$

where:

$$\bar{T} = \frac{1}{2}\int_0^{\bar{L}_1}\left(\frac{\partial \bar{y}_1}{\partial \bar{t}}\right)^2 \mathrm{d}\bar{x}_1 + \frac{1}{2}\int_0^{1-\bar{L}_1}\left(\frac{\partial \bar{y}_2}{\partial \bar{t}}\right)^2 \mathrm{d}\bar{x}_2$$

$$\begin{aligned} \bar{V} = {} & \frac{1}{2}\int_0^{\bar{L}_1}\left(\frac{\partial^2 \bar{y}_1}{\partial \bar{x}_1^2}\right)^2 \mathrm{d}\bar{x}_1 + \frac{1}{2}\int_0^{1-\bar{L}_1}\left(\frac{\partial^2 \bar{y}_2}{\partial \bar{x}_2^2}\right)^2 \mathrm{d}\bar{x}_2 \\ & + \frac{1}{2}\bar{k}_r\left[\left.\frac{\partial \bar{y}_1}{\partial \bar{x}_1}\right|_{\bar{x}_1=\bar{L}_1} - \left.\frac{\partial \bar{y}_2}{\partial \bar{x}_2}\right|_{\bar{x}_2=0}\right]^2 \\ & + \frac{1}{2}\bar{k}_s[\bar{y}_1|_{\bar{x}_1=\bar{L}_1} - \bar{y}_2|_{\bar{x}_2=0}]^2 \end{aligned}$$

$$\bar{W}_c = \frac{1}{2}\int_0^{\bar{L}_1} \bar{P}_1\left(\frac{\partial \bar{y}_1}{\partial \bar{x}_1}\right)^2 \mathrm{d}\bar{x}_1 + \frac{1}{2}\int_0^{1-\bar{L}_1} \bar{P}_2\left(\frac{\partial \bar{y}_2}{\partial \bar{x}_2}\right)^2 \mathrm{d}\bar{x}_2$$

$$\delta\bar{W}_{nc} = -\bar{P}_0\left(\left.\frac{\partial \bar{y}_2}{\partial \bar{x}_2}\right|_{\bar{x}_2=1-\bar{L}_1}\right)\delta\bar{y}_2|_{\bar{x}_2=1-\bar{L}_1} + \bar{F}_0(\bar{t})\delta\bar{y}_2|_{\bar{x}_2=\bar{x}_{F_0}} \tag{8}$$

The non-dimensional axial forces are:

$$\begin{cases} \bar{P}_1 = \bar{P}_0\bar{x}_1, & 0 \leqslant \bar{x}_1 \leqslant \bar{L}_1 \\ \bar{P}_2 = \bar{P}_0(\bar{L}_1 + \bar{x}_2), & 0 \leqslant \bar{x}_2 \leqslant 1-\bar{L}_1 \end{cases} \tag{9}$$

Considering the fact that the axial force distribution on the beam is not constant, the governing differential equation cannot be solved analytically and an approximation method must be used. Ritz method is the one that has been employed in this study using Hamilton's principle. In this method, the response is approximated with a series as the following:

$$\begin{cases} \bar{y}_1(\bar{x}_1, \bar{t}) = \sum_{i=1}^{N} \varphi_{1i}(\bar{x}_1) q_i(\bar{t}) \\ \bar{y}_2(\bar{x}_2, \bar{t}) = \sum_{i=1}^{N} \varphi_{2i}(\bar{x}_2) q_i(\bar{t}) \end{cases} \tag{10}$$

$\varphi_i(\bar{x})$ is admissible function and $q_i(\bar{t})$ is a generalized coordinate. By replacing the above series in Eqs. (7) and (8), the following simplified matrix form can be derived:

$$\lfloor \mathbf{M}_{ij} \rfloor \lfloor \ddot{\mathbf{q}}_j \rfloor + \lfloor \mathbf{K}_{ij} \rfloor \lfloor \mathbf{q}_j \rfloor = \lfloor \mathbf{Q}_j \rfloor \tag{11}$$

where $\ddot{q} = \mathrm{d}^2 q/\mathrm{d}t^2$, $\lfloor \mathbf{M}_{ij} \rfloor$ is the mass matrix, $\lfloor \mathbf{K}_{ij} \rfloor$ is the stiffness matrix and $\lfloor \mathbf{Q}_j \rfloor$ is the generalized force vector and can be described as:

$$\begin{aligned} \mathbf{M}_{ij} = {} & \int_0^{\bar{L}_1} \varphi_{1i}\varphi_{1j}\,\mathrm{d}\bar{x}_1 + \int_0^{1-\bar{L}_1} \varphi_{2i}\varphi_{2j}\,\mathrm{d}\bar{x}_2 \\ \mathbf{K}_{ij} = {} & \int_0^{\bar{L}_1} \varphi''_{1i}\varphi''_{1j}\,\mathrm{d}\bar{x}_1 + \int_0^{1-\bar{L}_1} \varphi''_{2i}\varphi''_{2j}\,\mathrm{d}\bar{x}_2 \\ & + \bar{k}_r\big[\varphi'_{1i}(\bar{L}_1) - \varphi'_{2i}(0)\big]\big[\varphi'_{1j}(\bar{L}_1) - \varphi'_{2j}(0)\big] \\ & + \bar{k}_s\big[\varphi_{1i}(\bar{L}_1) - \varphi_{2i}(0)\big]\big[\varphi_{1j}(\bar{L}_1) - \varphi_{2j}(0)\big] \\ & - \bar{P}_0\left[\int_0^{\bar{L}_1} \bar{x}_1\varphi'_{1i}\varphi'_{1j}\,\mathrm{d}\bar{x}_1 + \int_0^{1-\bar{L}_1} (\bar{L}_1 + \bar{x}_2)\varphi'_{2i}\varphi'_{2j}\,\mathrm{d}\bar{x}_2\right] \\ & + \bar{P}_0\varphi'_{2i}(1-\bar{L}_1)\varphi_{2j}(1-\bar{L}_1) \\ \mathbf{Q}_j = {} & \bar{F}_0(\bar{t})\varphi_{2j}(\bar{x}_{F_0}) \end{aligned} \tag{12}$$

for $i, j = 1, 2, \ldots, N$ where $\varphi' = \mathrm{d}\varphi/\mathrm{d}\bar{x}$ and $\varphi'' = \mathrm{d}^2\varphi/\mathrm{d}\bar{x}^2$.

As it is shown in the above equation, the partial differential equation is converted to a set of ordinary differential equations using the approximation method.

2.2. Admissible functions

In general the admissible function should satisfy four conditions:

1. At least must satisfy all geometric boundary conditions.
2. Must be continuous and differentiable to highest spatial derivative.
3. Should be a complete function.
4. Must be linearly independent.

The mode shapes of a free–free jointed bipartite beam satisfy the above conditions and have been used in this study. As the first two rigid body modes are not involved in instability, they are not considered as the admissible functions. It is to be noted that the rigid body modes are controlled by the force in the transverse direction, to be considered in the simulation to be followed.

$$\begin{cases} \varphi_1(\bar{x}_1) = A_1 \sin(\lambda\bar{x}_1) + A_2 \cos(\lambda\bar{x}_1) + A_3 \sinh(\lambda\bar{x}_1) \\ \qquad\qquad + A_4 \cosh(\lambda\bar{x}_1), \quad 0 \leqslant \bar{x}_1 \leqslant \bar{L}_1 \\ \varphi_2(\bar{x}_2) = A_5 \sin(\lambda\bar{x}_2) + A_6 \cos(\lambda\bar{x}_2) + A_7 \sinh(\lambda\bar{x}_2) \\ \qquad\qquad + A_8 \cosh(\lambda\bar{x}_2), \quad 0 \leqslant \bar{x}_2 \leqslant 1 - \bar{L}_1 \end{cases} \tag{13}$$

$A_1, \ldots, A_8$ are mode shape coefficients. And:

$$\lambda^4 = \frac{mL^4}{EI}\omega_i^2 \tag{14}$$

ω_i is the natural frequency of the free–free jointed bipartite beam. The boundary conditions in the assumed model are:

$$\begin{cases} \varphi_1''(0) = 0, \quad \varphi_1'''(0) = 0 \\ \varphi_2''(1-\bar{L}_1) = 0, \quad \varphi_2'''(1-\bar{L}_1) = 0 \\ \varphi_1''(\bar{L}_1) = \varphi_2''(0) = \bar{k}_r\big[\varphi_1'(\bar{L}_1) - \varphi_2'(0)\big] \\ \varphi_1'''(\bar{L}_1) = \varphi_2'''(0) = \bar{k}_s\big[\varphi_1(\bar{L}_1) - \varphi_2(0)\big] \end{cases} \tag{15}$$

where $\varphi''' = \mathrm{d}^3\varphi/\mathrm{d}\bar{x}^3$.

3. Rigid body motion and control strategy

The transfer function is first obtained from the rigid body equations for the pitch canal, as described below. The control design for the actuator oscillations is then described.

3.1. Modeling of the pitch channel in the FLV

For modeling the pitch channel of the FLV in which the elastic behavior follows Eq. (11), one can demonstrate these vibrational effects only in the IMU [6]. Hence, the IMU senses the rigid pitch angle associated with the dynamics of rigid motion as well as the elastic pitch angle associated with Eq. (11). This statement similarly holds for the rate of the pitch angle as shown in Fig. 2. The slope of the bending vibration deflection can be found by

$$\theta_b = \frac{\partial y(x_{IMU}, t)}{\partial x} = \sum_{i=1}^{N} \varphi_i'(x_{IMU}) q_i(t) \tag{16}$$

where $\varphi_i'(x_{IMU})$ is the slope of the mode shape at the IMU location and θ_b is the magnitude of the bending angle. The total pitch magnitude θ_T is equal to the sum of the pitch magnitude of a rigid beam (θ) and the bending angle. This is expressed as

$$\theta_T = \theta + (-\theta_b) \tag{17}$$

The negative sign in Eq. (17) is related to the particular frames used. The dynamics of rigid body is stated with the derivation of the equation of motion for the flight device in the standard format. These equations for the pitch channel in the linear form lead to a third order transfer function. The transfer function between the actuator deflection of the pitch channel (δ_p) and θ is given in the following equation:

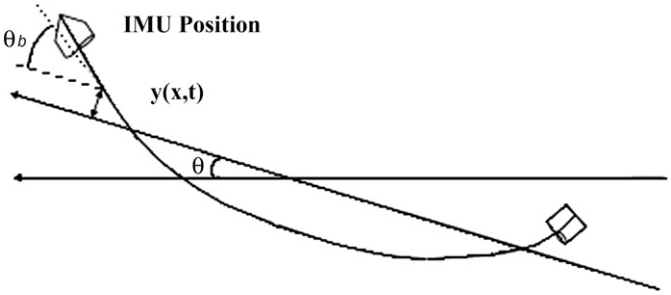

Fig. 2. Calculation of total pitch angle associated with rigid and elastic motion.

$$\frac{\theta}{\delta_p} = \frac{-b_1 s + (a_1 b_1 - a_2 b_2)}{s(s^2 - (a_3 + a_4)s + (a_3 a_4 - a_5 a_6))} \tag{18}$$

where a_i and b_j are related to the aerodynamic and system dynamic relations.

3.2. The main approach to control the actuator oscillations

The main strategy to prevent the destructive effects of TSTO LV vibrations is to filter the structural dynamics excitation in the closed loop of the rigid control system. In the structures controlled by a closed loop, there are internal excitation sources as well as the external ones that could affect the control system. The internal excitation sources are of vital importance because the continuous interaction of the actuators and the measuring systems, and involving the vibration of the structure, cause the instability or high oscillation on the actuators. This phenomenon can obviously found in TSTO LVs.

To prevent such destructive effects, the main approach developed in this study is to protect the vibrational bias from feeding back into the control system. In another word, it is desirable that the measuring devices do not sense the bending vibration and do not send any excitation feedback to the actuators in all conditions. For this purpose, the vibrational excitation exclusion includes two steps: estimation of the bending vibration frequencies, and filtering these frequencies. As the vibration frequencies vary in respect to the time, the challenging issue is to estimate them. The approach used in this paper to estimate the bending frequencies is filtered recursive least square (FRLS).

Many different filtering methods are available and can be used to filter bending vibrations such as low pass, high pass and notch filtering. A special kind of notch filtering has been employed in this research. A simplified infinite impulse response notch filter can be expressed as follows:

$$H(z) = \frac{A(z)}{B(z)} = \frac{1 + 2\alpha z^{-1} + z^{-2}}{1 + \alpha(1+\beta)z^{-1} + \beta z^{-2}} \tag{19}$$

where α is a function of the center frequency of the filter and β is a constant parameter. Because eight vibration modes of the elastic beam model of TSTO LV are considered in this study, for first guest, it seems that eight series of filters must be used to reduce the vibrational effects. But as the first and the second vibration modes are the most active modes and the other ones are in low amplitude, only two filters can be employed in the control loop with good accuracy. Moreover, in respect to bandwidth of closed loop element such as actuator and linear controller, in all conditions, only the main mode of the system dominantly affects on the performance of the system. All of these considerations have led the

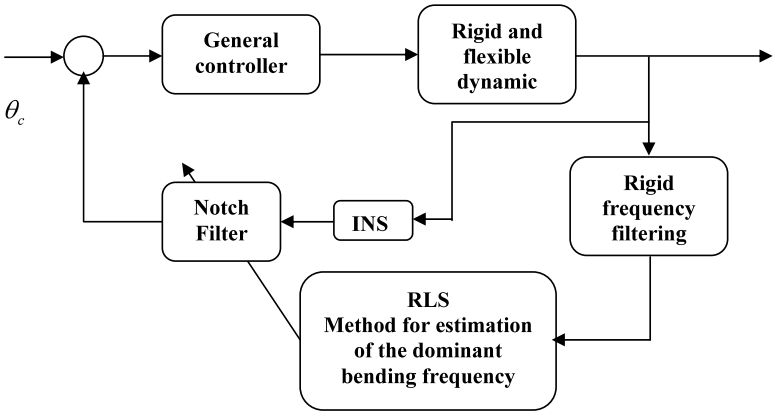

Fig. 3. The adaptive algorithm and the control loop.

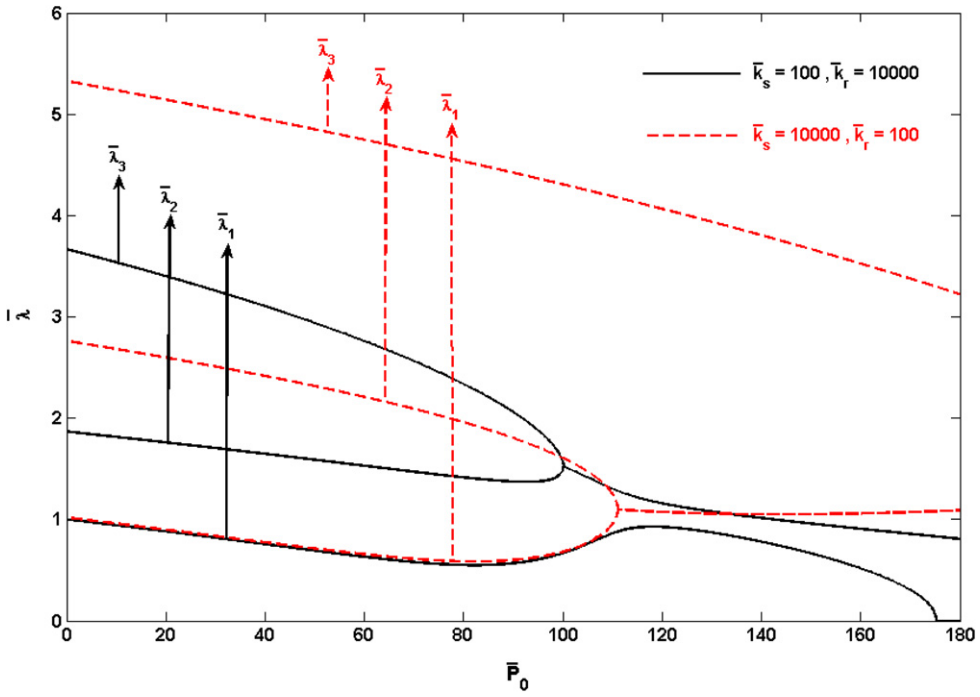

Fig. 4. Variations of the first, the second and the third non-dimensional natural frequencies versus the non-dimensional follower force $\bar{P}_0$ for particular values of $\bar{k}_r$ and $\bar{k}_s$ when $\bar{L}_1 = 0.4$.

study to design only one adaptive filter, even though that the system consists of more vibration modes. This claim is considerably shown and discussed in later sections of this paper.

3.3. FRLS method

The dynamic model of TSTO LV consist of rigid and elastic parts, hence, applying the RLS method for estimating the bending frequency lead to high volume of calculations and processes. On the other hand, it is assumed that the parameters of rigid body dynamic in the flight time are known. Considering this assumption for reducing the volume of process, one can eliminate the rigid body model in estimation algorithm by using FRLS method.

In FRLS method by eliminating the rigid body dynamic in the estimation algorithm and considering the elastic dynamic as a linear second order model, it can implement an algorithm for only estimating the vibrational parameters such as the bending frequency. This algorithm can tune the center frequency of the notch filter for reducing the vibrational effect in the main control loop. The block diagram for this method is shown in Fig. 3.

If the input of the first filter for eliminating the rigid body dynamic is $u(n)$ at the nth step and output of the pole section is $g(n)$:

$$g(n) = \frac{1}{B(z)}u(n) \tag{20}$$

Then, the output of the filter $w(n)$ can be expressed as:

$$w(n) = g(n) + 2\alpha g(n-1) + g(n-2) \tag{21}$$

With regard to equations of RLS method and the parameters introduced above, the basic equations of FRLS can be expressed as follow:

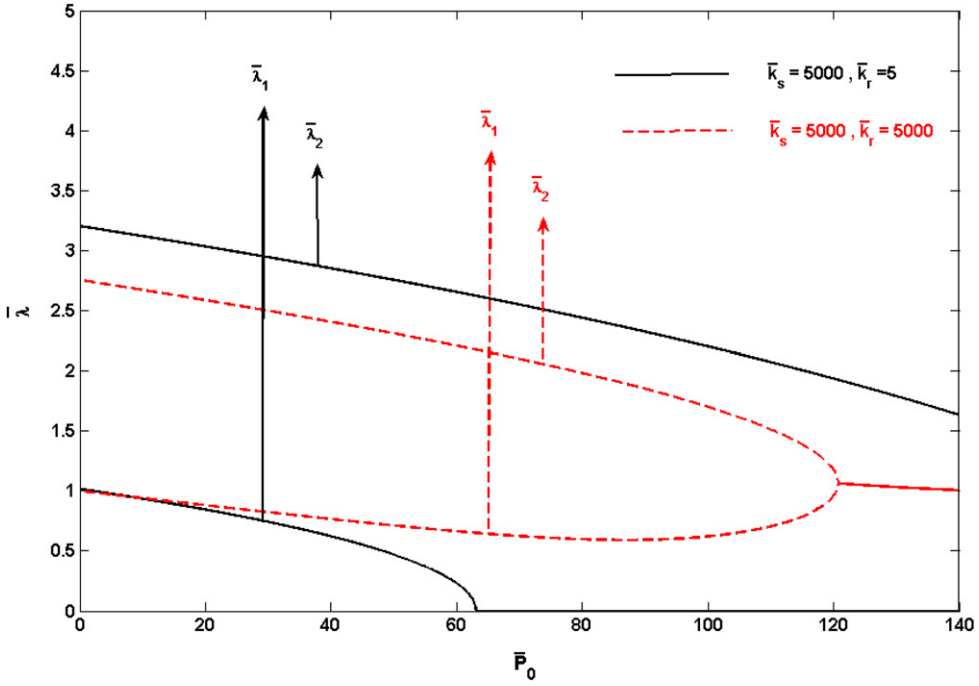

Fig. 5. Variations of the first and second non-dimensional natural frequencies versus the non-dimensional follower force $\bar{P}_0$ for two sets of $\bar{k}_r$ and $\bar{k}_s$ when $\bar{L}_1 = 0.8$.

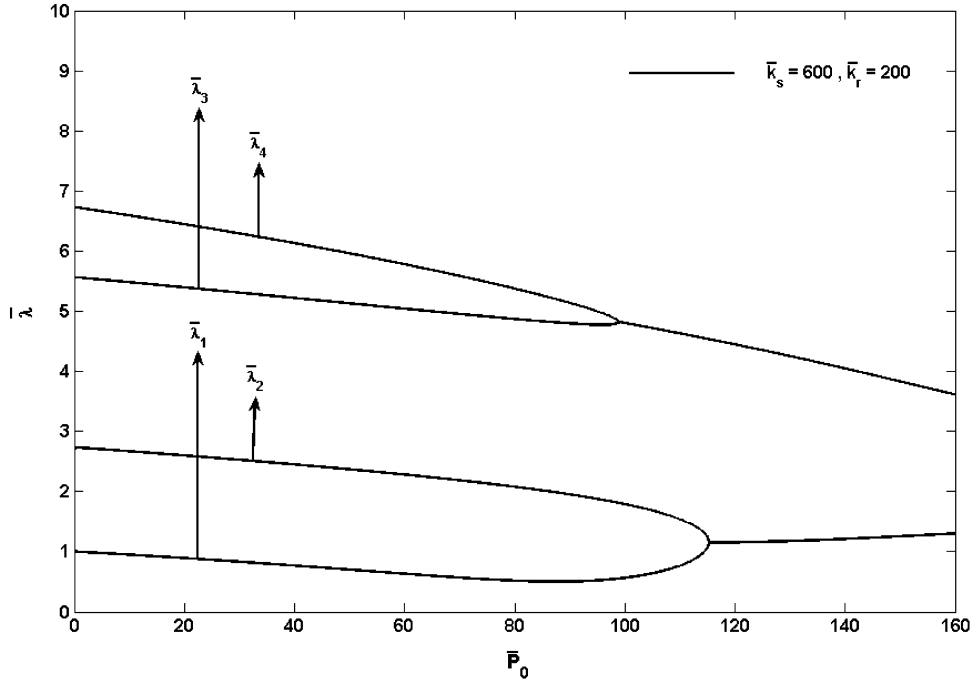

Fig. 6. The first instability occurs because of the convergence of the third and the forth natural frequencies when $\bar{k}_r = 200$, $\bar{k}_s = 600$ and $\bar{L}_1 = 0.8$.

$$\hat{z}(n) = \hat{z}(n-1) + k_{cg}(n)\big[w(n) - \psi^T(n)\hat{z}(n-1)\big]$$
$$k_{cg}(n) = \eta(n-1)\psi(n)\big[I + \psi^T(n)\eta(n-1)\psi(n)\big]^{-1}$$
$$\eta(n) = \big[I - k_{cg}(n)\psi^T(n)\big]\eta(n-1) \tag{22}$$

where $\hat{z}(n)$ is the estimated parameters matrix, $k_{cg}(n)$ is the correcting gain, I is the identity matrix, $\psi(n)$ and $\eta(n)$ are recursive parameters and regression model of output, respectively. The dominant bending vibration frequency in any condition is a function of the parameters of elastic dynamic, therefore by accurate estimating of these parameters the bending frequency is accurately estimated.

4. Numerical results and discussion

4.1. Critical follower force

In this research, the effects of the location of the joint on the critical follower force ($\bar{P}_{0cr}$) were analyzed by choosing four dif-

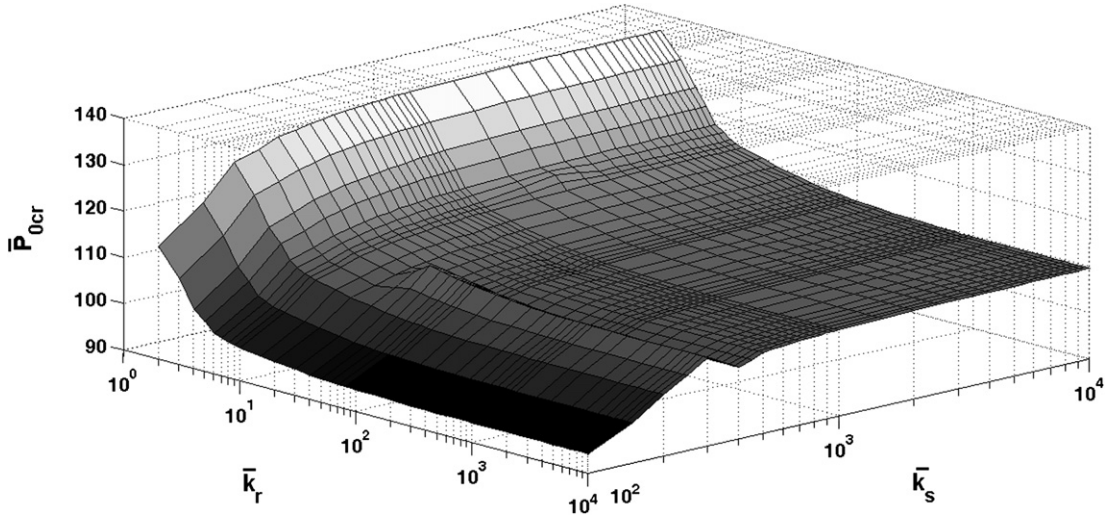

Fig. 7. The effects of variation of $\bar{k}_r$ and $\bar{k}_s$ on the non-dimensional critical follower force ($\bar{P}_{0cr}$) when $\bar{L}_1 = 0.2$.

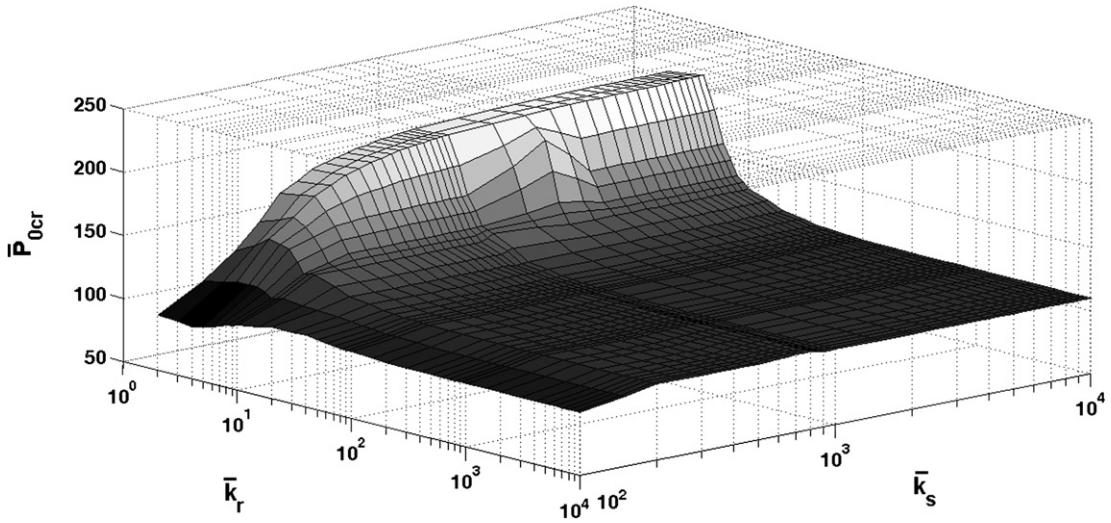

Fig. 8. The effects of variation of $\bar{k}_r$ and $\bar{k}_s$ on the non-dimensional critical follower force ($\bar{P}_{0cr}$) when $\bar{L}_1 = 0.4$.

ferent location i.e. $\bar{L}_1 = 0.2, 0.4, 0.6, 0.8$. Also the effects of the stiffness of the spring joints are investigated by changing $\bar{k}_r$ from 10^0 to 10^4 and $\bar{k}_s$ from 10^2 to 10^4. One of the aims of this work is to find the first or the lowest critical follower force $\bar{P}_0$ which cause the instability in the system. It is worth mentioning that only the first four natural frequencies were investigated for this purpose. And the number of mode shapes used for the Ritz method is 8 ($N = 8$). To obtain the variation of the natural frequencies by the follower force, one needs to set the right hand side of Eq. (11) to zero ($\bar{F}_0(\bar{t}) = 0$) and assumes that the homogeneous response is in form of:

$$[\mathbf{q}_j] = [\bar{\mathbf{q}}_j]e^{i\bar{\lambda}\bar{t}}, \quad i = \sqrt{-1}, \quad \bar{\lambda} = \frac{\lambda}{\lambda_1} \tag{23}$$

where $[\bar{\mathbf{q}}_j]$ is a constant vector, and λ_1 is the first natural frequency for $\bar{P}_0 = 0$. So, $\bar{\lambda}$ is the non-dimensional frequency of the system with non-zero of $\bar{P}_0$. The critical follower force is very dependent to the joint location and the springs stiffness. These parameters also affect the type and characteristics of the instability from divergence to flutter or vice versa. In the flutter regime, the joint location and the springs stiffness also change the cause of the flutter from merging the first and the second natural frequencies to merging the second and the third one, or the third and the forth one. For example, some cases have been shown in Figs. 4, 5 and 6.

4.1.1. *Case* $\bar{L}_1 = 0.2$

For the case $\bar{L}_1 = 0.2$, the joint is located at one fifth of the beam from the top. The results of this research for this case show that for all of the values of $\bar{k}_r$ and $\bar{k}_s$, the dominant instability is flutter and is due to the convergence of the first and the second natural frequencies. In Fig. 7 the effects of variation of $\bar{k}_r$ and $\bar{k}_s$ on the non-dimensional critical follower force are presented.

4.1.2. *Case* $\bar{L}_1 = 0.4$

When $\bar{L}_1 = 0.4$, the joint is located at two fifth of the beam from the top. The results for this case show that for all of the values of $\bar{k}_r$ and $\bar{k}_s$, still the dominant instability is flutter and is mostly due to the convergence of the first and the second natural frequencies. Only when $\bar{k}_s$ is low and $\bar{k}_r$ is high then the second and the third natural frequencies converge and flutter happens. In Fig. 8 the effects of variation of $\bar{k}_r$ and $\bar{k}_s$ on the non-dimensional critical follower force ($\bar{P}_{0cr}$) are presented.

4.1.3. *Case* $\bar{L}_1 = 0.6$

The results for this case show some interesting results. When the joint location gets closer to the end (where the follower force is applied) the instability can occurs due to divergence (the first natural frequency becomes zero) or flutter (due to the convergence of the first and the second natural frequencies) depending to the

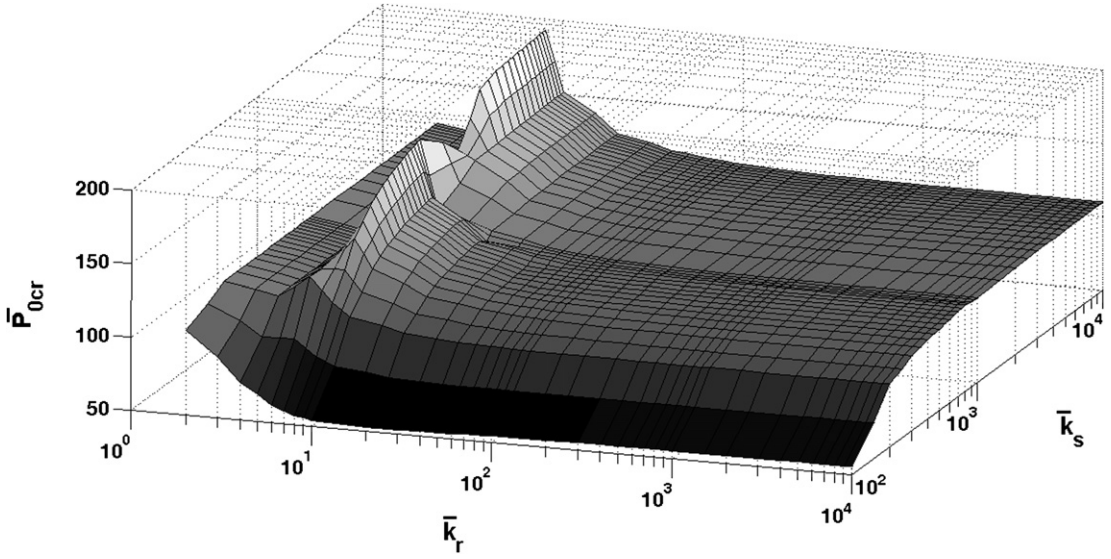

Fig. 9. The effects of variation of $\bar{k}_r$ and $\bar{k}_s$ on the non-dimensional critical follower force ($\bar{P}_{0cr}$) when $\bar{L}_1 = 0.6$.

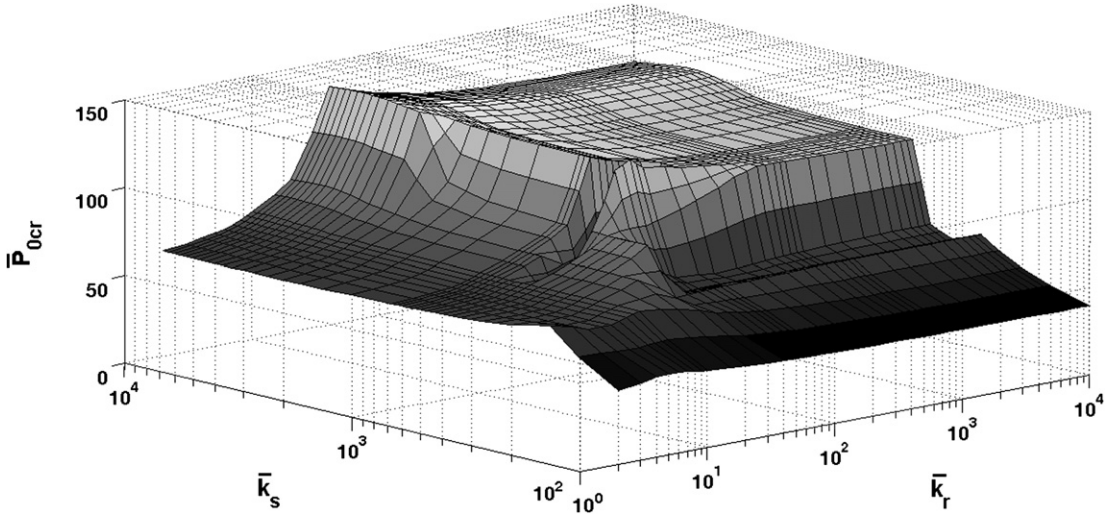

Fig. 10. The effects of variation of $\bar{k}_r$ and $\bar{k}_s$ on the non-dimensional critical follower force ($\bar{P}_{0cr}$) when $\bar{L}_1 = 0.8$.

values of springs stiffness. In fact for small values of $\bar{k}_r$ the first natural frequency decreases when the follower force is increased and becomes zero (divergence). But when $\bar{k}_r$ has higher values the dominant mode of instability becomes flutter. In Fig. 9 the effects of variation of $\bar{k}_r$ and $\bar{k}_s$ on the non-dimensional critical follower force ($\bar{P}_{0cr}$) are presented.

The sharp risen section of Fig. 9 is the border between divergence instability (small values of $\bar{k}_r$) and the flutter instability (higher values of $\bar{k}_r$). For a constant value of $\bar{k}_s$, the critical follower force in divergence in this case is less than the one in flutter. Also when the flutter is the dominant instability mode, and $\bar{k}_r$ increases, the critical follower force decreases. It means that instability happens with lower values of the follower force.

4.1.4. Case $\bar{L}_1 = 0.8$

The results for this case show that when the joint location gets near to the end (where the follower force is applied) the instability can occur unpredictably due to divergence (the first natural frequency becomes zero) or flutter (due to the convergence of the first and the second or the third and the forth natural frequencies) depending to the values of springs stiffness. In Fig. 10, the effects of variation of $\bar{k}_r$ and $\bar{k}_s$ on the non-dimensional critical follower force ($\bar{P}_{0cr}$) are presented. The main reason for the plunge in the surface is that for some values of $\bar{k}_r$ and $\bar{k}_s$, the first instability occurs when the third and the forth natural frequencies are converged.

To verify the current results, when the joint of the bipartite beam is in high stiffness, it should represent approximately a uniform beam and the critical follower force both models should be close to each other. This fact could be clearly found in Figs. 7, 8, 9 and 10. When the values of $\bar{k}_r$ and $\bar{k}_s$ are increasing, the value of critical follower force of this model is close to the value of critical follower force of uniform beam ($\bar{P}_{0cr} = 109.9$, Beal).

4.2. Displacement analysis

One of the aims of this research is to analyze the displacement of a point in the beam near the tip where normally the Inertial Measuring Units (IMU) is located. The analysis of displacements and vibrations of this point over the time is crucial for any control system used in the aerospace structure. The point is shown in Fig. 1 and its distance to the tip of the beam is x_{IMU}.

For calculating the vibration in IMU position, one can use Eqs. (1), (2) and (3) instead of Eqs. (7), (8) and (9). The advan-

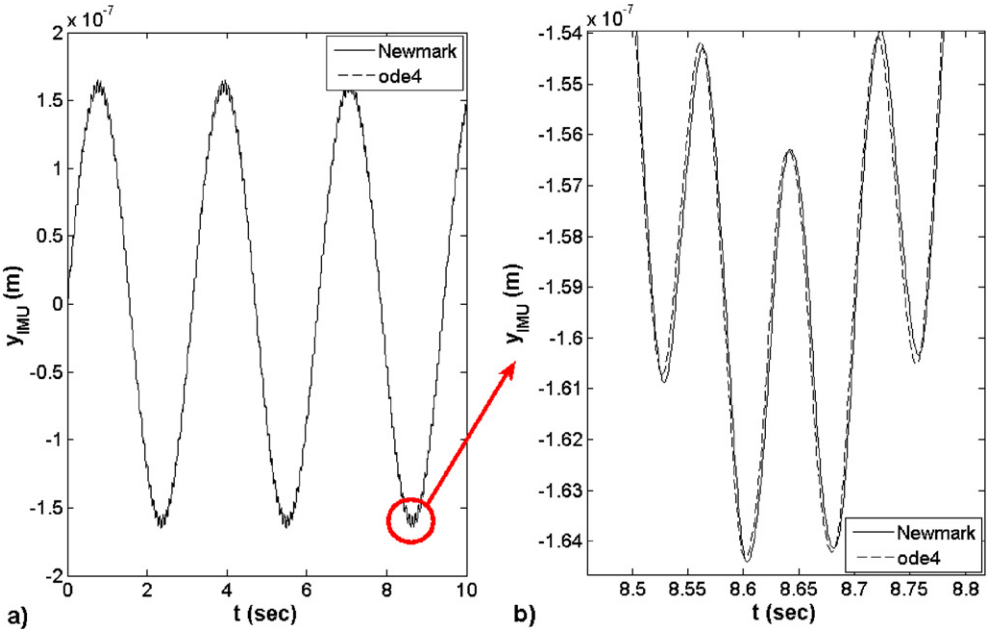

Fig. 11. (a) Displacement of the location of IMU. (b) A detailed comparison of results from Newmark and ode4 methods.

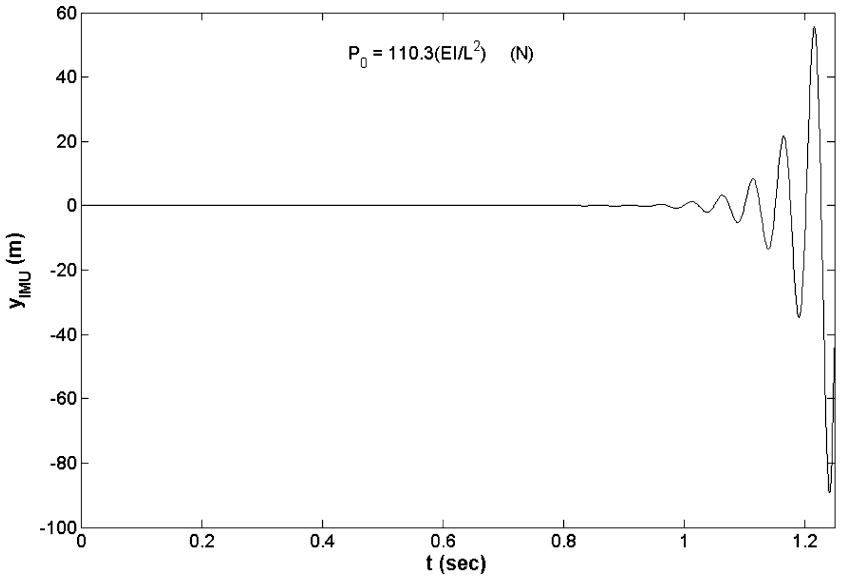

Fig. 12. The effects of an over critical follower force on the displacement of IMU.

tage of this selection is to use dimensional parameters which have been non-dimensional in the previous section.

In Fig. 11(a) the deflection of the location of IMU (i.e. $y(x_{IMU}, t)$) is calculated using Newmark and ode4 (Runge–Kutta Formula) methods, and the results are compared in Fig. 11(b). One example is selected for this analysis which is: $x_{IMU} = 0.2 \times L_1$, $x_{F_0} = L_2$, $k_s = 3000 \times (EI/L^3)$ and $k_r = 3000 \times (EI/L)$. The first instability for this case ($L_1 = 4$ m, $L_2 = 16$ m, $EI = 8.1997 \times 10^{10}$ N m^2) is flutter and happens when $P_0 = 109.3 \times (EI/L^2)$ N. It is also assumed that $P_0 = 50 \times (EI/L^2)$ N and $F(t) = 100 \times \sin(2t)$ N.

Fig. 12 shows that for the same controller force as previous examples ($F(t) = 100 \times \sin(2t)$ N) if the follower force is more than the critical one (for example $P_0 = 110.3 \times (EI/L^2)$ N), the amplitude of the displacement increases rapidly with time.

4.3. Simulation

In this section the effects of the follower force on the controller loop are investigated and analyzed. As Figs. 13(a) and 13(b) show, the slope of IMU location and the angle of the actuator increases over the time when the follower force is critical ($P_0 = 109.3 \times (EI/L^2)$ N). The angle of the actuator becomes saturated because the flutter phenomenon happened in the structure.

The outcome resulted by applying the adaptive control on the system for $P_0 = 108.3(EI/L^2)$ N (which is less than the critical follower force) is shown in Figs. 14 to 16. Fig. 14 presents the frequency estimation using the adaptive algorithm. As shown in this figure, the adaptive algorithm estimates the main active frequency in the TSTO LV vibration properly and the error in recognized frequency is low and acceptable. The variations of the angle of the

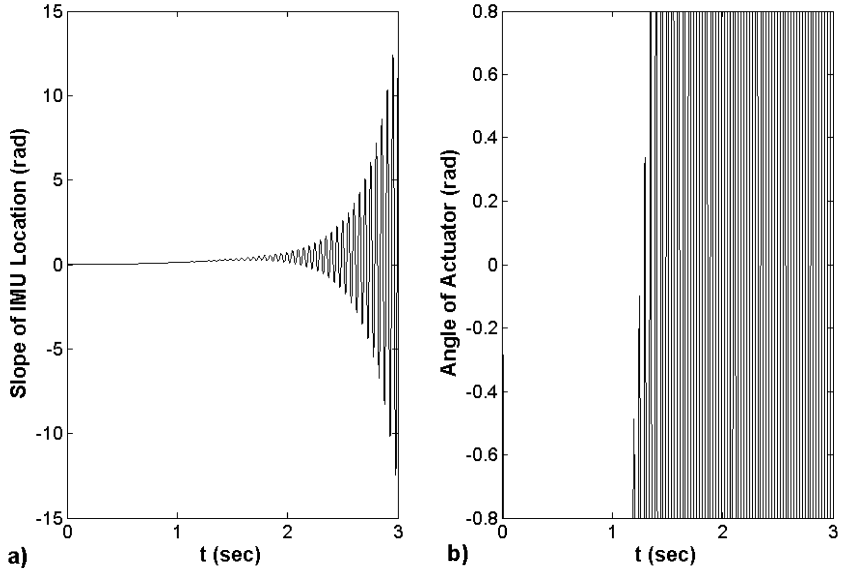

Fig. 13. (a) The slope of IMU location versus time. (b) The angle of actuator versus time.

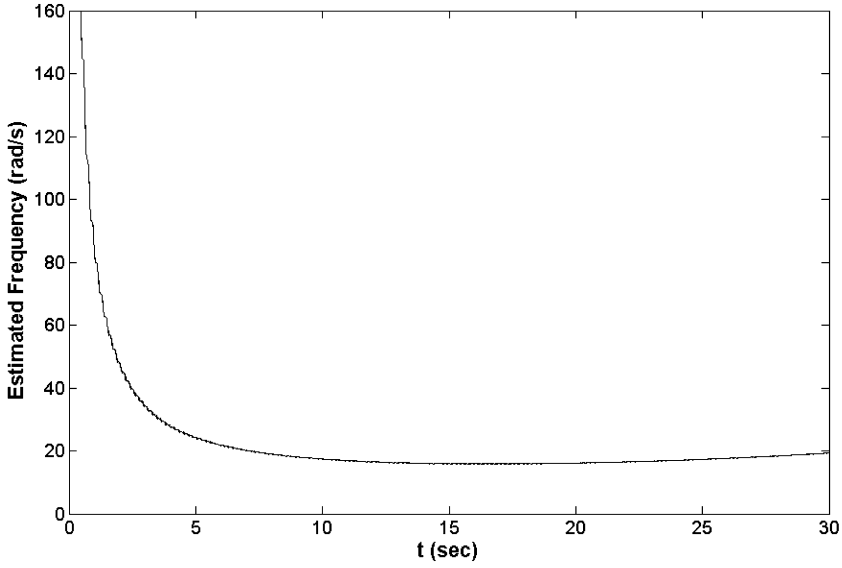

Fig. 14. The frequency estimation using the adaptive algorithm.

actuator in two cases (with and without adaptive controller) are shown in Fig. 15. The oscillation of the actuator is obviously reduced when the adaptive controller is applied. Fig. 16 shows the variations of the angle of the IMU in the system while the adaptive control system is applied and also is compared with the same variations without controller. Fig. 16 shows that the controller was able to converge the vibration of the IMU while it was divergent when no controller was applied.

5. Conclusions

In this paper, the instability and vibrations of a free–free jointed bipartite Bernoulli beam under the follower and transversal forces, TSTO LV structure, are analyzed that is a model for such structures with propulsion and controller (actuator) forces (the actuator forces responsible for the control and guidance of the TSTO LV). The follower force is the representative of the propulsion force and the transversal force is modeled the controller force. Two parts of the beam are jointed by two rotational ($\bar{k}_r$) and shear springs ($\bar{k}_s$). The variations of stiffness of the springs would change the critical follower force as well as the type of the instability unpredictably as shown in Section 4.1. The results show that the dominant instability of the beam is flutter when the joint is located in the top half of the beam. As the joint location gets down to the half, the third natural frequency is also playing an important role in the flutter instability as shown in case $\bar{L}_1 = 0.4$. When the joint location is in the second half, i.e. $\bar{L}_1 = 0.6$ and $\bar{L}_1 = 0.8$, both divergence and flutter become the instability modes. In the case $\bar{L}_1 = 0.6$, flutter occurs due to the convergence of the first and the second natural frequencies only. When the joint location gets closer to the beam end (where the follower force is applied), flutter could also happens due to the convergence of the third and the forth natural frequencies. The results of this paper offer an approximation method to design the joint location and springs for a free–free jointed bipartite Bernoulli beam under the follower force.

The destructive effects of the bending vibration of a TSTO LV (when the follower force is considered) on its control system and especially on the undesirable oscillations of its actuator are also studied. In this work, the equations of motion of elastic bending vibration of the TSTO LV having a follower force is derived and

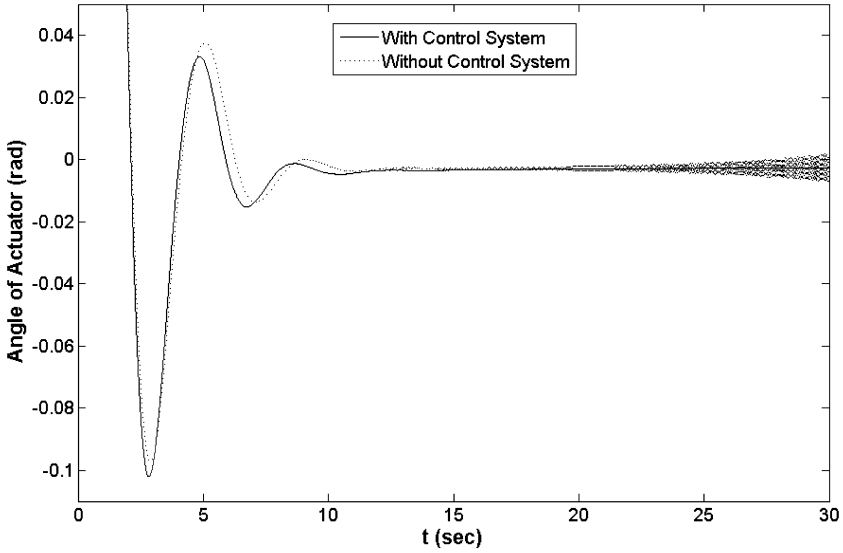

Fig. 15. The variations of the angle of the actuator in two cases (with and without adaptive controller).

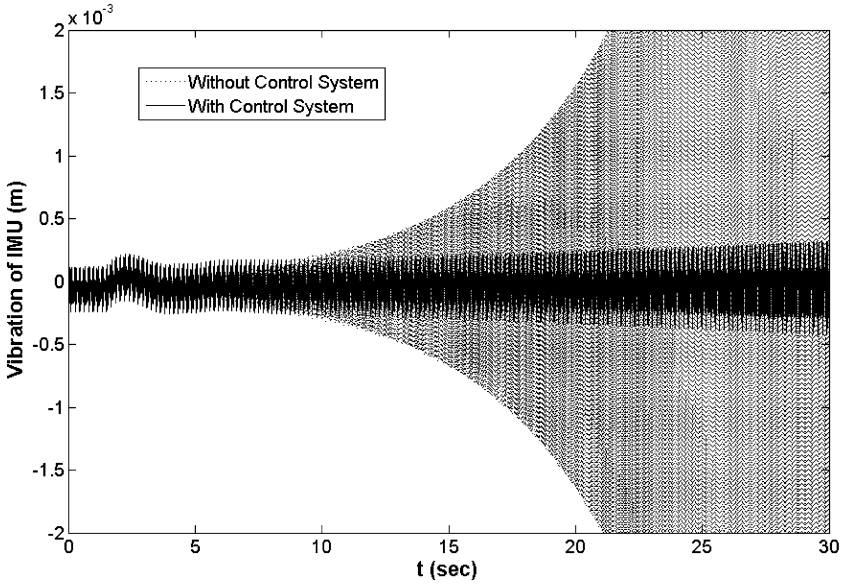

Fig. 16. Comparison of the vibration of IMU position in the system with and without adaptive controller.

added to a control system. It has been shown that the effects of the bending vibration on oscillations of the actuators are of vital importance and when the follower force is increased the oscillation of the actuators also increases considerably. To reduce these negative effects, the bending vibration of the TSTO LV was modeled using the eight mode shapes and regarding to the only one dominant frequency of system, and an adaptive notch filter could almost omit the bending vibration of the IMU location from the control system. The results of the current work show that this strategy which has been successfully employed in the models without any follower force influences, can reduce the negative effects of the structural vibrations especially in the presence of any follower force effects. Finally, in this paper it is illustrated with applying such as system one can design a TSTO LV with its maximum follower force and control the high amplitude vibration of the IMU location.

References

[1] F.T.K. Au, D.Y. Zheng, Y.K. Cheung, Vibration and stability of non-uniform beams with abrupt changes of cross-section by using C^1 modified beam vibration functions, Applied Mathematical Modelling 29 (1999) 19–34.

[2] T.R. Beal, Dynamic stability of a flexible missile under constant and pulsating thrusts, AIAA Journal 3 (3) (1965) 486–494.

[3] J. Bibel, H. Stalford, An improved gain stabilized mu-controller for a flexible launch vehicle, AIAA-92-0206, in: 30th Aerospace Sciences Meeting & Exhibit, January 6–9, 1992, NV, pp. 1–16.

[4] J. Bibel, H. Stalford, Mu-synthesis autopilot design for a flexible launch vehicle. AIAA-19371, in: 29th Aerospace Sciences Meeting, January 7–10, 1991, Nevada, pp. 1–17.

[5] A. Bokaian, Natural frequencies of beam under compressive axial loads, Journal of Sound and Vibration 126 (1) (1988) 49–65.

[6] H.D. Choi, H. Bang, An adaptive control approach to the attitude control of a flexible rocket, Control Engineering Practice 8 (2000) 1003–1010.

[7] H.D. Choi, J. Kim, Adaptive notch filter design for bending vibration of a sounding rocket, Aerospace Engineering Journal of IMechE 215 (2000) 13–23.

[8] F.M. Detinko, Lumped damping and stability of Beck column with a tip mass, International Journal of Solids and Structures 40 (2003) 4479–4486.

[9] A. Di Egidio, A. Luongo, A. Paolone, Linear and non-linear interactions between static and dynamic bifurcations of damped planar beams, International Journal of Non-Linear Mechanics 42 (2007) 88–98.

[10] M.J. Englehart, J.M. Krause, An adaptive control concept for flexible launch vehicles, AIAA-92-4622-CP, 1992, pp. 1505–1512.

[11] P.A. Hassanpour, W.L. Cleghorn, J.K. Mills, E. Esmailzadeh, Exact solution of the oscillatory behavior under axial force of a beam with a concentrated mass within its interval, Journal of Vibration and Control 13 (12) (2007) 1723–1739.

[12] S. Irani, O. Kavianipour, Effects of a flexible joint on instability of a free–free jointed bipartite, Journal of Zhejiang University Science A 10 (9) (2009) 1252–1262.
[13] K.W. Jenkins, R.J. Roy, Pitch control of a flexible launch vehicle, IEEE Transaction on Automatic Control (Short papers) (1968) 181–186.
[14] A. Joshi, Free vibration characteristics of variable mass rocket having large axial thrust/acceleration, Journal of Sound and Vibration 187 (4) (1995) 727–736.
[15] O. Kavianipour, S.H. Sadati, Effects of damping on the linear stability of a free–free beam subjected to follower and transversal forces, Structural Engineering and Mechanics 33 (6) (2009) 709–724.
[16] A.M. Khoshnood, J. Roshanian, A. Khaki-sedigh, Model reference adaptive control for a flexible launch vehicle, Journal of Systems and Control Engineering 222 (1) (2007) 45–52.
[17] J.H. Kim, Y.S. Choo, Dynamic stability of a free–free Timoshenko beam subjected to a pulsating follower force, Journal of Sound and Vibration 216 (4) (1998) 623–636.
[18] M.A. Langthjem, Y. Sugiyama, Optimum shape design against flutter of a cantilevered column with an end-mass of finite size subjected to a non-conservative load, Journal of Sound and Vibration 226 (1) (1999) 1–23.
[19] M.A. Langthjem, Y. Sugiyama, Dynamic stability of columns subjected to follower loads: a survey, Journal of Sound and Vibration 238 (5) (2000) 809–851.
[20] Jun-Seok Lee, Nam-Il Kim, Moon-Young Kim, Sub-tangentially loaded and damped Beck's columns on two-parameter elastic foundation, Journal of Sound and Vibration 306 (2007) 766–789.
[21] M.C. Maki, J. Van De Vegte, Optimal and constrained-optimal control of a flexible launch vehicle, AIAA Journal 10 (6) (1972) 796–799.
[22] L. Meirovitch, Principles and Techniques of Vibrations, Prentice-Hall International, Inc., New Jersey, United States of America, 1997.
[23] K.A. Mladenov, Y. Sugiyama, Stability of a jointed free–free beam under end rocket thrust, Journal of Sound and Vibration 199 (1) (1997) 1–15.
[24] G.C. Nihous, On the continuity of boundary value problem for vibrating free–free straight beams under axial loads, Journal of Sound and Vibration 200 (1) (1997) 110–119.
[25] C.S. Oh, H. Bang, C.S. Park, Attitude control of a flexible launch vehicle using an adaptive notch filter: Ground experiment, Control Engineering Practice 16 (2008) 30–42.
[26] Y.P. Park, Dynamic stability of a free Timoshenko beam under a controlled follower force, Journal of Sound and Vibration 113 (3) (1987) 407–415.
[27] Y.P. Park, C.D. Mote Jr., The maximum controlled follower force on a free–free beam carrying a concentrated mass, Journal of Sound and Vibration 98 (2) (1984) 247–256.
[28] S.H. Pourtakdoust, N. Assadian, Investigation of thrust effect on the vibrational characteristics of flexible guided missiles, Journal of Sound and Vibration 272 (2004) 287–299.
[29] E.G. Ryanski, Optimal control of flexible launch vehicle, AIAA paper, No. 67-592, in: Guidance, Control and Flight Dynamics Conference, Huntsville, Alabama, August 14–16, 1967, pp. 1–7.
[30] Si-Ung Ryu, Y. Sugiyama, Computational dynamics approach to the effect of damping on stability of a cantilevered column subjected to a follower force, Computers and Structures 81 (2003) 265–271.
[31] K. Sato, On the governing equation for vibrating and stability of a Timoshenko beam: Hamilton's Principle, Journal of Sound and Vibration 145 (2) (1991) 338–340.
[32] Y. Sugiyama, M.A. Langthjem, Physical mechanism of the destabilizing effect of damping in continuous non-conservative dissipative systems, International Journal of Non-Linear Mechanics 42 (2007) 132–145.
[33] J.J. Wu, On the stability of a free–free beam under axial thrust subjected to directional control, Journal of Sound and Vibration 43 (1) (1975) 45–52.